Environ. Sci. Technol. **2005**, *39,* 4793−4800

Organic and Inorganic Aerosol Below-Cloud Scavenging by Suburban New Jersey Precipitation

STEVEN F. MARIA† AND LYNN M. RUSSELL*,‡

SciTec, Inc., Princeton, New Jersey 08540, and Scripps Institution of Oceanography, University of California San Diego, La Jolla, California 92093

Ambient aerosol size distributions and chemical composition in Princeton, NJ, were measured during a 10-day period in August 2003. Ten precipitation events during the sampling period maintained low aerosol concentrations, with an average gravimetric $PM_{1.0}$ of $8.2 \pm 1.6\ \mu g\ m^{-3}$ and an average Fourier transform infrared (FTIR) spectroscopy-measured $PM_{1.0}$ of $8.6 \pm 0.8\ \mu g\ m^{-3}$. A constrained factor analysis shows that the measured aerosol composition data are consistent with coal combustion and motor vehicle emissions. FTIR spectroscopy shows that the alkene fraction of organic mass (OM) was larger in the aerosol samples dominated by motor vehicle emissions than in the samples dominated by coal combustion, but the solvent-rinsing behavior was unaffected by source type. The aerosol OM was hydrophilic throughout the sampling period, with an average of 52% ± 10% of the identified OM removed in the water-rinsing stage of the FTIR analysis. Measurements before and after rain events showed changes in particle composition and number distribution that were used to characterize the rate and chemical selectivity of particle removal processes associated with precipitation (or, in general terms, scavenging). The changes in ambient particle distributions showed an average $PM_{1.0}$ below-cloud scavenging coefficient of $7 \times 10^{-5} \pm 3 \times 10^{-5}\ s^{-1}$, with variability associated with chemical composition. The fraction of the aerosol OM removed in water rinses decreased during rain events, typically 55% at the start and 30% at the end of the observed rain events. These measured chemically dependent removal rates are consistent with other field measurements and can be used to improve the description of aerosol lifetimes in global models.

Introduction

Wet and dry deposition of aerosol particles are important removal mechanisms that maintain a balance between atmospheric sources and sinks. Wet removal by precipitation is the more efficient process, responsible for an estimated 86% of the total deposition of atmospheric aerosol sulfate (*1*), and can occur through nucleation scavenging or impaction scavenging. Nucleation scavenging is the dominant in-cloud aerosol scavenging mechanism and involves aerosol particles acting as condensation nuclei during cloud droplet formation. Impaction scavenging depends on the relative motion of an aerosol particle and a cloud or rain droplet, is relevant both in-cloud and below-cloud, and is believed to be the dominant scavenging mechanism for below-cloud aerosol particles (*2*). Impaction scavenging has been modeled by use of scavenging coefficients that are functions of rain intensity and particle size, independent of aerosol composition (*3*).

The independence of below-cloud particle removal and composition is an assumption that has not been verified in field observations. Measurements of pre- and post-rain aerosol concentrations in the boundary layer allow for characterization of the chemical evolution of airborne aerosol particles during precipitation, quantifying below-cloud particle removal mechanisms. In this manner, scavenging coefficients have previously been measured in remote regions as a function of rain intensity (*4*, *5*). Such measurements have been subject to large variability and have lacked simultaneous chemical measurements, causing aerosol wet removal processes to remain a large source of uncertainty in aerosol transport models (*6*).

Field measurements in Princeton, NJ, during August of 2003 provide chemical and physical aerosol data from which we derived boundary-layer below-cloud scavenging coefficients during multiple rain events and their relationship to chemical composition. Fourier transform infrared (FTIR) spectroscopy and X-ray fluorescence (XRF) measurements, together with aerosol size distributions, are assembled here to provide a complete picture of aerosol source type, organic mass (OM) composition, and scavenging coefficients.

Experimental Section

During a 10-day period from 4 to 14 August 2003, aerosol dry size distributions and chemical composition were measured from the roof of Fine Hall (55 m above ground level, 90 m above sea level, 40.347° N, 74.652° W, corner of Washington Road and Ivy Lane) on the Princeton University campus in Princeton, NJ. Sample air was drawn in from underneath an inverted-funnel rain-hat to prevent rain droplets from entering the sampling lines.

Size Distribution Measurement. Aerosol dry diameters were measured with an aerodynamic particle sizer (APS, TSI Incorporated, Shoreview, MN, model 3320) and a differential mobility analyzer (DMA, TSI Inc., Shoreview, MN, models 3071a and 3010), both downstream of diffusion dryers. The APS collected size distributions for 0.5−20 μm diameter particles. The DMA, with a sheath flow of 4.3 L min^{-1} and a flow ratio of 1:10, classified particles into 60 logarithmically distributed size channels between the diameters of 0.01 and 0.6 μm. A complete aerosol size distribution was collected every 10 min throughout the sampling period. Aerosol losses in the tubing upstream of the APS and DMA were minimized by using conductive silicone tubing for aerosol lines.

FTIR and XRF Measurements. A separate aerosol sample stream pulled 40 L min^{-1} through diffusion dryers and then through an impactor with a cut point (d_{50}) of 1 μm. Downstream of the impactor, a 10 L min^{-1} sidestream was separated out and pulled through two 37 mm diameter Teflon filters in series (Pall Corp., Ann Arbor, MI, 1 μm Teflon) that were masked down to 10 mm diameter by use of Teflon gaskets. Five Teflon filter samples were collected from sunrise to sunset each day, and one filter sample was collected each night, with the following filter-changing schedule: 0600 h, 0845 h, 1130 h, 1415 h, 1700 h, and 1945 h. At 1945 h each day, the pumps were shut down for 15 min while the spent desiccant in the diffusion dryers was replaced with fresh desiccant. The nighttime filter sample was then started at

* Corresponding author e-mail: lmrussell@ucsd.edu.
† SciTec, Inc.
‡ Scripps Institution of Oceanography.

10.1021/es0491679 CCC: $30.25
Published on Web 05/18/2005

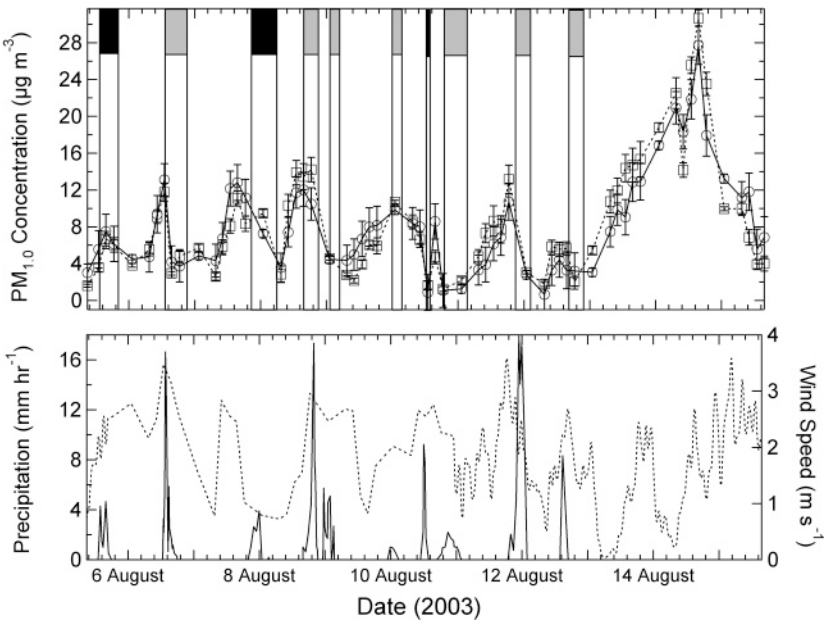

FIGURE 1. (Top panel) Submicrometer aerosol mass concentrations measured gravimetrically (○, —) and by summing all identified FTIR species (□, ---). Error bars indicate measurement uncertainties. Rain events measured by an independent weather station in Princeton, NJ, are shown as gray or black filled areas and vertically extending lines. The black rain events meet conservative criteria for determining that rain scavenging is the dominant aerosol particle removal mechanism and were used to calculate scavenging coefficients (see text for explanation). (Bottom panel) Precipitation rates (—) and wind speeds (---) throughout the sampling period.

2000 h each evening. After sampling, solvent-rinsed FTIR measurements were performed on these filters as described by Maria et al. (*7*, *8*) to quantify particulate species including sulfate ions, ammonium ions, nitrate ions, carbonate carbon, silicate ions, organic carbon (OC), organic mass (OM), and organic functional groups (alkane, alkene, aromatic, carbonyl, alcohol, amine, and organosulfate). Particulate nitrate was below detection limits in 85% of the aerosol samples and composed less than 1% of the total measured aerosol mass in the remaining aerosol samples. Solvent-rinsing was performed with four solvents in the following order: hexane, dichloromethane, acetone, and water. Sixty-three Teflon filter samples were analyzed for chemical composition in this manner, and all Teflon filters were preweighed and post-weighed to determine a gravimetric aerosol mass. XRF measurements were also performed on 21 of these filters as described by Maria et al. (*7*).

Results and Discussion

Ten rain events maintained low aerosol concentrations throughout the 10-day sampling period, with an average gravimetric $PM_{1.0}$ of 8.2 ± 1.6 $\mu g\ m^{-3}$ and an average FTIR-measured $PM_{1.0}$ of 8.6 ± 0.8 $\mu g\ m^{-3}$. These two measurements deviated from each other by an average of 1.2 $\mu g\ m^{-3}$ during the sampling period but were only significantly different from each other for nine of the 63 aerosol samples. In the complete time series, shown in Figure 1, there is a strong correlation between the two methods of determining $PM_{1.0}$. Also visible in Figure 1 is the reduction in aerosol concentrations during and immediately following each rain event.

FTIR-measured $PM_{1.0}$ is the sum of identified OM, sulfate, ammonium, silicate, and carbonate concentrations. OM is determined from the absorption signatures of alkane C−H, alkene C−H, aromatic C−H, carbonyl C═O, alcohol C−OH, amine C−N, and organosulfate C−O−S bonds in the infrared spectral region (*8*). These organic functional group measurements cannot account for highly branched organic compounds that consist primarily of C−C bonds but have been shown to accurately predict OM with an error of less than 5% for gas chromatography/mass spectrometry- (GCMS-) identified atmospheric OM speciations (*9*). The SO_4^{2-} υ_1 symmetrical stretch, the NH_4^+ deformation, the O−Si−O asymmetrical stretch of SiO_4^{4-}, and the CO_3^{2-} asymmetrical stretch are used respectively to quantify sulfate, ammonium, silicate, and carbonate ions in aerosol samples. For these inorganic species, the absorbance signatures rigorously hold only for the ions in a solvated state or in an ionic compound such as $(NH_4)_2SO_4$ (ammonium sulfate) or Na_4SiO_4 (sodium silicate). The crystalline quartz and kaolinite silicate complexes have asymmetrical stretches that are shifted to 1090 and 1010 cm^{-1}, respectively, from the 1035 cm^{-1} absorbance of the silicate ion (*10*, *11*). Such shifts away from the infrared wavenumber used for quantification result in reduced sensitivities of the analysis method to large complexes such as quartz and kaolinite. The wavenumber shifts associated with quartz and kaolinite do not cause significant errors in measurements of combustion-related submicrometer aerosol samples that contain very small dust concentrations.

Gravimetric measurements include the mass of all aerosol components, including possible contributions from sea salt, trace elements, or particulate water that FTIR does not detect. The agreement of gravimetric and FTIR-measured $PM_{1.0}$ mass concentrations within the range of experimental uncertainties is an indication that seasalt, trace elements, non-silicate dust species, and water were responsible for a small fraction of the aerosol mass for the majority of this sampling campaign. XRF-derived concentrations of trace elements (Al, K, Ca, Ti, V, Cr, Mn, Fe, Co, Ni, Cu, Zn, Ga, Ge, As, Se, Br, Rb, Sr, Y, Zr, Mo, Ag, In, Pb, and a lower bound of sea salt from Cl) averaged 0.5% of the FTIR-measured $PM_{1.0}$ and were always below 1.6% of the FTIR-measured $PM_{1.0}$. For the nine samples with significant disagreements between the FTIR and gravimetric measurements, the FTIR measurement was larger (four samples) or smaller (five samples) than the gravimetric measurement. A smaller FTIR measurement may indicate the presence of sea salt or non-silicate dust, and a larger FTIR measurement may indicate the presence of species with larger-than-average absorptivities in the quantified infrared regions. The agreement is comparable to the 14% average

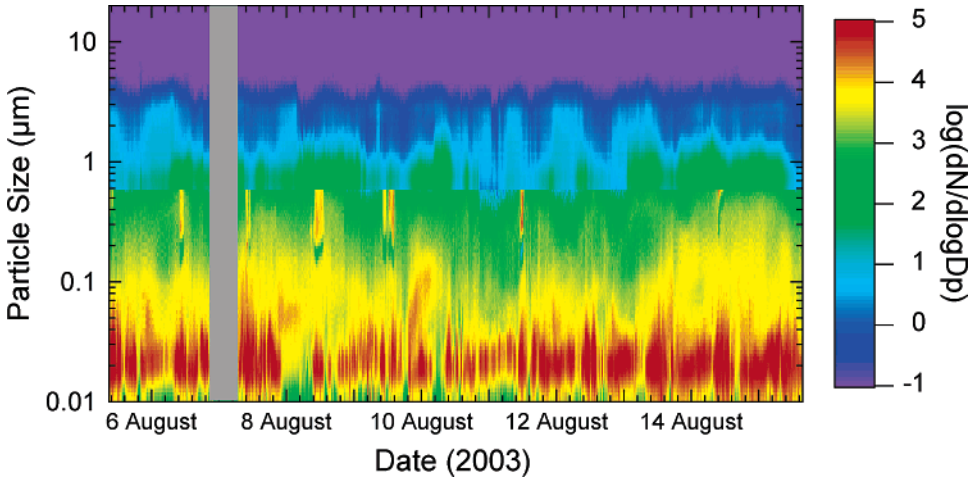

FIGURE 2. Aerosol number distributions measured in Princeton, NJ, with a temporal resolution of 10 min. DMA measurements are used for particle dry diameters in the range of 0.01−0.55 μm, and APS measurements are used for dry diameters in the range of 0.55−20 μm. The gray filled area represents missing data.

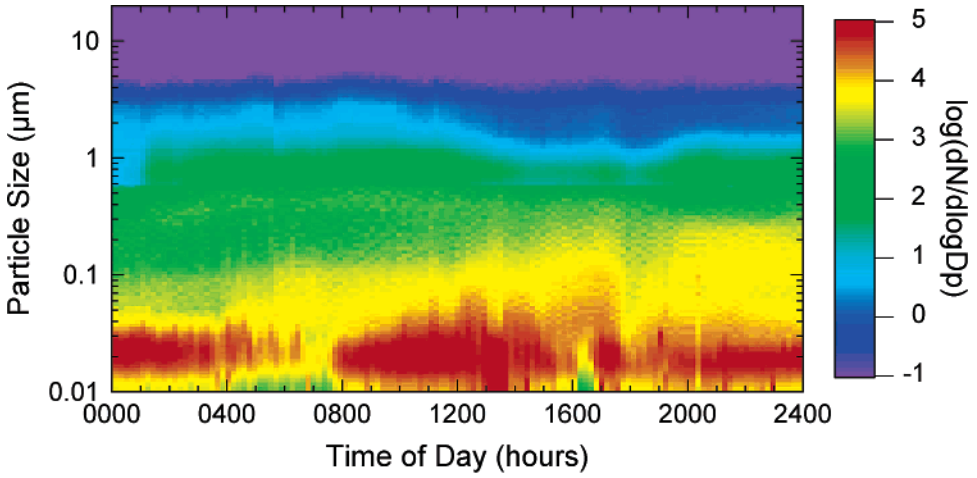

FIGURE 3. Aerosol number distributions measured in Princeton, NJ, on 13 August 2003 with a temporal resolution of 10 min. DMA measurements are used for particle diameters in the range of 0.01−0.55 μm, and APS measurements are used for diameters in the range of 0.55−20 μm.

discrepancy of recent submicrometer mass closure studies by a combination of ion chromatography, particle-induced X-ray emissions spectroscopy, and thermal−optical carbon analysis to determine the chemical composition (*12*, *13*).

Throughout the sampling period, peaks in the aerosol number distributions occurred at diameters of 0.02−0.03 μm, as seen in Figure 2. These Aitken mode particles account for 75% of the submicrometer aerosol number distribution but only 1% of the submicrometer aerosol volume distribution. Second peaks at ~0.4 μm are also visible in Figure 2, at approximately 1200 h on 6, 7, 8, 9, and 11 August 2003 and lasting for 1−4 h each. These accumulation mode peaks occurred only when the meteorology was between rain events, consistent with a scenario in which the rain events are washing out the majority of the aerosol particles in this size range. On 13 August 2003, when there was no rain event, the aerosol size distribution developed throughout the day as shown in Figure 3. A small average wind speed of 1.2 m s^{-1} and a consistent aerosol composition throughout the day (42% ± 4% sulfate, 10% ± 2% ammonium, and 48% ± 4% OM) both suggest that changes in the aerosol size distributions were not caused by changes in air mass. From 0700 to 1800 h, the size distribution broadened from a peak near 0.02 μm to a distribution spanning 0.01−0.3 μm. The initial peak broadening occurred rapidly, with the peak maximum increasing from 0.03 to 0.07 μm in approximately 2 h. This particle growth can be explained by coagulation or secondary aerosol production that was not observable on days with rain events. Modeled back trajectories show the air mass arriving onshore from the Atlantic Ocean approximately 2 h prior to collection, suggesting local sources for the aerosol particles since there were no significant combustion sources on the Atlantic Ocean. Local sources included a nearby natural gas power plant and major roadways.

Constrained Factor Analysis. Henry et al. (*14*) found that a sample size of at least 62 is preferred in order to perform a factor analysis on a data set with 20 chemical species. Due to the small size of the current data set, with complete FTIR and XRF chemical information for only 21 samples, a traditional factor analysis could not be performed on the data. Instead, a constrained factor analysis, in which the factors were prespecified, was performed on the 21 samples for which XRF data were available. The predetermined factors were taken from the analysis by Lee et al. (*15*) of 8 years of data from Brigantine, NJ (1991−1999), only ~65 miles southeast of the Princeton sampling site. Species with uncertainties higher than 50% of their average values were not included in the constrained factor analysis, leaving the following species: OC (15% uncertainty), sulfate (21% uncertainty), silicate (17% uncertainty), K (19% uncertainty), Ca (30 uncertainty), Fe (18% uncertainty), and Zn (30% uncertainty).

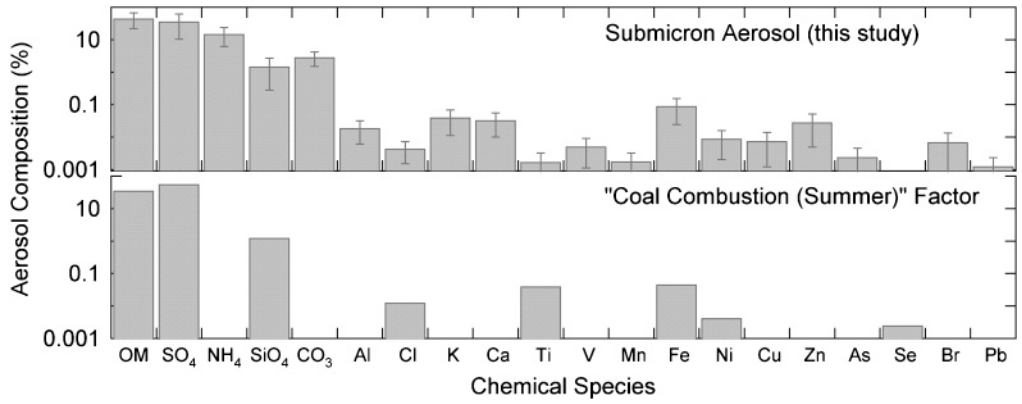

FIGURE 4. Average percentage composition of all aerosol samples collected in Princeton, NJ, with standard deviations shown as error bars. Also shown is the composition of the "coal combustion (summer)" factor from Lee et al. (*15*).

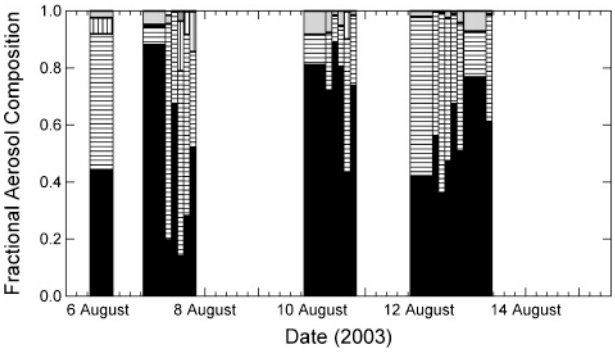

FIGURE 5. Factor contribution to aerosol in Princeton, NJ, as determined by using the factors of Lee et al. (*15*) in a constrained factor analysis. Shown from bottom to top are the coal combustion (summer) factor (black bars), the motor vehicle/mixed combustion factor (horizontally striped bars), the diesel/Pb−Zn factor (vertically striped bars), the waste incineration factor (dark gray bars), the sea salt factor (light gray bars), and the soil factor (white bars).

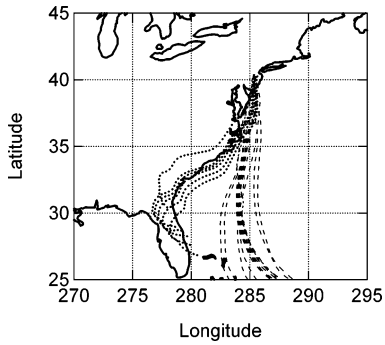

FIGURE 6. Five-day back trajectories at the sampling altitude and location calculated by use of the HYSPLIT$_4$ model (*16*) for 7 August 2003 (···) and 10−12 August 2003 (---). Trajectories up to 5000 m above sea level show similar paths.

The results of the constrained factor analysis reveal that on average the coal combustion (summer) factor accounts for 57% of the measured aerosol mass. Lee et al. (*15*) report that the coal combustion (summer) factor was responsible for 60% of their fine aerosol mass, similar to what was shown in the measurements in this study. The average measured submicrometer aerosol composition is shown in Figure 4, along with the composition of the coal combustion (summer) factor. The large contribution of this factor to aerosol mass explains the high fraction of sulfate (36%) in the aerosol. It should be noted that the coal combustion (summer) factor of Lee et al. (*15*) is indicative not of pure coal emissions but of a mixed and aged atmospheric aerosol that contains tracers associated with coal combustion.

The important role of the coal combustion (summer) factor is consistent with the majority of back trajectories (*16*) passing directly over the coal combustion source regions identified by Lee et al. (*15*) just a few hours prior to sampling. The second largest contributor to the aerosol (37%) is the motor vehicle/mixed combustion factor, in contrast to the aerosol measured at Brigantine. This difference is explained by the close proximity of the Princeton sampling site to major highways. The remaining minor contributors to the measured aerosol were calculated to be the diesel/Pb−Zn (3%), sea salt (2%), waste incineration (0.3%), and soil (0.2%) factors.

Deviations from the average aerosol factor composition were observed throughout the 10-day period and are shown as a complete time series in Figure 5. Measured mass fractions on 7 August 2003 have large values for the motor vehicle/mixed combustion and diesel/Pb−Zn factors. At midday, the mass fractions are 65% and 18%, respectively, with a contribution of only 14% from the coal combustion (summer) factor. Compared to 7 August 2003, at 1200 h on 12 August 2003 there was a larger influence from the coal combustion (summer) factor (47%) and a smaller influence from the motor vehicle/mixed combustion (50%) and diesel/Pb−Zn (0.1%) factors. These differences are partially explained by differences in back trajectories, as shown in Figure 6. Back trajectories followed the Eastern coast of the United States until 9 August 2003, while after that date the back trajectories arrived from further out over the ocean. This increased contact with populated regions and mobile sources prior to 9 August 2003 is consistent with the increased factor contribution from mobile sources on 7 August 2003 as compared to 10 and 12 August 2003. The New Jersey sampling site is 40 miles inland from the ocean, and the air masses that arrived from the Atlantic Ocean after 9 August 2003 were over land for 2 h prior to sampling.

Organic Functional Group Composition. The FTIR-identified functional groups, like the factor analysis results and the back trajectories, varied between the beginning and end of the 10-day sampling period. Organic alkene functional groups comprised 24% ± 7% of OM before 9 August 2003 as compared to only 11% ± 4% of OM after 9 August 2003, as seen in Figure 7. Alkane and amine functional groups were larger fractions of OM near the end of the project, comprising 69% ± 6% and 0.04% ± 0.2% OM, respectively, before 9 August 2003 compared to 81% ± 7% and 0.5% ± 1.4% OM after 9 August 2003. Unlike alkene, alkane, and amine functional groups, the OM fractions of aromatic, alcohol, carbonyl, and organosulfate groups were not significantly different between the beginning and end of the sampling period.

The change in OM composition at 9 August 2003 coincides with the change in calculated factor composition noted above.

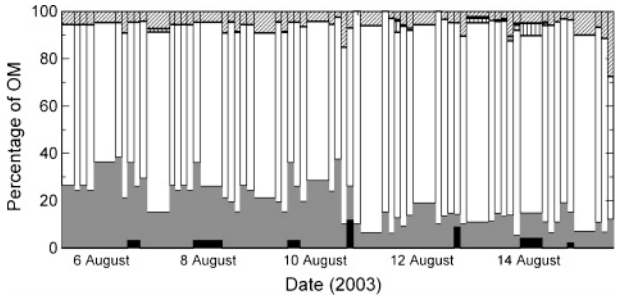

FIGURE 7. Fractional organic mass in Princeton, NJ, aerosol samples. Shown, from bottom to top, are the contributions from aromatic (black), alkene (gray), alkane (white), amine (vertically striped), organosulfur (horizontally striped), alcohol (checkered), and carboxyl (diagonally striped) functional groups.

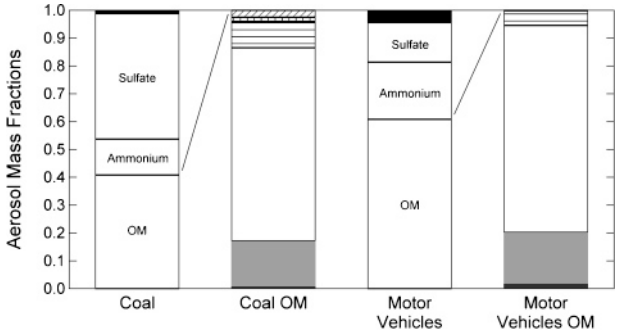

FIGURE 8. Fractional $PM_{1.0}$ and OM compositions for aerosol samples dominated by the coal combustion (summer) and motor vehicle/mixed combustion factors. For $PM_{1.0}$, black regions indicate the mass fractions of dust and trace elements. For OM, shown from bottom to top are the contributions from aromatic (dark gray), alkene (light gray), alkane (white), carbonyl (horizontally striped), organosulfur (vertically striped), and amine (diagonally striped) functional groups. Alcohol functional groups were below the detection limit in the samples shown here. Particulate nitrate did not compose more than 1% of aerosol mass for these samples.

The period with larger alkene OM fractions and smaller alkane and amine OM fractions corresponds to the period that was largely influenced by motor vehicle/mixed combustion and diesel/Pb−Zn factors. A comparison of chemical compositions for the coal combustion (summer) and motor vehicle/mixed combustion factors is shown in Figure 8, where the compositions are averages of all aerosol samples with 75% or more of aerosol mass from the corresponding factor. This comparison suggests that motor vehicle or diesel emissions of OM have a larger fraction of alkene and smaller fractions of alkane and amine than coal combustion emissions do. This result is consistent with ion chromatography (IC) source measurements, because for automobile and diesel truck sources IC has only identified ~5% of the total particle-phase OC (*17*, *18*). FTIR measurements have been shown to identify nearly 100% of OC (*8*).

The OM rinsing behavior shows an average of 52% removal in the water rinse (a 52% water-soluble fraction of OM), both at the beginning and toward the end of the sampling period. The water rinse is the final stage of the rinsing process, so less than 50% of OM was removed in the prior hexane, dichloromethane, and acetone rinses. The observed compositional changes in the ratio of alkene to alkane, both nonpolar functional groups, did not affect the OM water solubility. This consistency in the rinsing behavior suggests that the concentration of polar functional groups (carbonyl and alcohol), which remained near 6% of OM throughout the sampling period, may be the controlling factor in determining water solubility. The 50% water-soluble OM fraction in Princeton is larger than fractions of 25% measured near Japan (*8*) and 43% measured in the Caribbean (*7*). Larger and more varied dust concentrations measured in the Caribbean and Japan and more highly variable carbonyl and alcohol concentrations (from 0% to 54% of OM) measured in Japan are both possible contributors to the observed differences in solvent rinsing behavior at these three locations.

Precipitation Scavenging. Aerosol particle losses during rain events were analyzed to determine below-cloud particle scavenging coefficients (λ) according to the method described by Laakso et al. (*5*). Briefly, the basic equation for the change in below-cloud aerosol concentration $c(d_p)$ due to rain scavenging is integrated from t_0 to t_1 to give

$$\lambda(d_p) = -\frac{1}{t_1 - t_0} \ln\left[\frac{c_1(d_p)}{c_0(d_p)}\right] \quad (1)$$

where $\lambda(d_p)$ is the size-dependent scavenging coefficient, $c_0(d_p)$ is the aerosol number concentration at t_0, and $c_1(d_p)$ is the aerosol number concentration at t_1. Equation 1 assumes that two consecutively measured air parcels had identical aerosol size distributions prior to the rain event and were exposed to rain at the same time. A change in air mass during the sampling period would affect the resulting calculated scavenging coefficient. Errors in the scavenging coefficient caused by instrumental errors, turbulence, advection, and particle growth during these measurement periods are assumed to be negligible.

By using only consecutive size distribution measurements ($t_1 - t_0 = 662$ s) during rain events with steady wind speeds of less than 3 m s^{-1}, constant wind direction, and rain intensity greater than 0.4 mm h^{-1} for longer than 0.5 h, changes in particle concentration caused by factors other than rain scavenging are minimized although not ruled out (*5*). Time periods without precipitation that meet all of the criteria for back trajectories, wind speed, and wind direction have an average rate of change (of absolute values of all increases and decreases) that varies between 5.9×10^{-6} and 1.4×10^{-5} s^{-1}. The upper bound of this range provides an estimate of the uncertainty in the derived scavenging coefficients. Since the measured decreases during precipitation exceed this upper bound by factors ranging from 2 to 10, there is strong evidence for a significant and different process occurring.

Three rain events satisfied the criteria of Laakso et al. (*5*): 1330−1645 h on 5 August 2003, 2040 h on 7 August through 0500 h on 8 August 2003, and 1300−1415 h on 10 August 2003 (marked in black in Figure 1). These three rain events all lasted for longer than 1 h, had rain intensities of greater than 3.2 mm h^{-1}, and had back trajectories that did not vary throughout each event. The resulting average size-dependent coefficients for each of these rain events are shown in Figure 9. The high relative humidity during these three rain events (RH > 98%) means that the wet diameters of the measured particles are at least a factor of 2 larger than the dry diameters, placing many of these aerosol particles into the size region where interception and impaction processes have efficiencies of greater than 10% (*3*, *19*).

The average $PM_{1.0}$ scavenging coefficient for these three rain events combined was $7 \times 10^{-5} \pm 3 \times 10^{-5}$ s^{-1}. This average coefficient is larger than the values reported by Laakso et al. (*5*) and Volken and Schumann (*4*) but smaller than the mean value of 2×10^{-4} s^{-1} reported by Claassen and Halm (*20*) for various sampling locations spanning the United States, Europe, and China. The average $PM_{1.0}$ scavenging coefficient for the rain event with a large influence from the coal combustion (summer) factor (10 August 2003 with a rain intensity of 8.0 mm h^{-1}) was 1.3×10^{-4} s^{-1}, 3.5 times larger than the average $PM_{1.0}$ scavenging coefficient for the two rain events with larger influences from the motor vehicle/

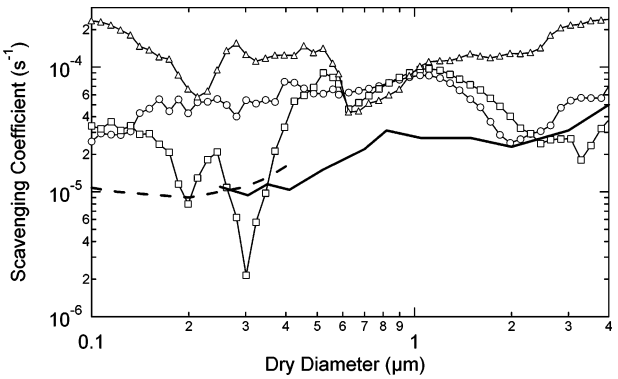

FIGURE 9. Measured scavenging coefficients for the rain events at 1330−1645 h on 5 August 2003 (○), 2040 h on 7 August through 0500 h on 8 August 2003 (□), and 1300−1415 h on 10 August 2003 (△). Also shown are the average field measurements of Laakso et al. (*5*) (− − −) and Volken and Schumann (*4*) (—).

mixed combustion factors (5 August 2003, with a rain intensity of 3.8 mm h^{-1} and an average scavenging coefficient of 4.9 × 10^{-5} s^{-1}; and 7−8 August 2003, with a rain intensity of 3.2 mm h^{-1} and an average scavenging coefficient of 2.8 × 10^{-5} s^{-1}). This significant difference in aerosol removal was observed despite the similar solvent-rinsing behavior of the pre-rain organic aerosol during these time periods.

Scavenging coefficients increase as rain intensity increases, and the larger rain intensity on 10 August 2003 may explain the larger scavenging coefficient observed on that day. Division of each scavenging coefficient by the average intensity of the corresponding rain event results in normalized coefficients of 6.0 × 10^{-2} mm^{-1} on 10 August, 4.7 × 10^{-2} mm^{-1} on 5 August, and 3.2 × 10^{-2} mm^{-1} on 7−8 August. The large variation in these normalized coefficients suggests that factors other than rain intensity may have influenced the aerosol removal rate. Source-dependent differences in the aerosol, such as the aerosol mixing state, composition, and age, may have also contributed to the differences in the observed below-cloud aerosol removal rates.

Laakso et al. (*5*) and Volken and Schumann (*4*) measured average scavenging coefficients with very little size dependence at remote European sampling sites. Scavenging coefficients in this study show strong size-dependent variations that are not explained by conventional models of impaction scavenging (*21*, *22*). Maxima and minima in the scavenging coefficient distributions in Figure 9 do not correspond to maxima or minima in the distributions of aerosol number or mass concentration, suggesting that heterogeneous particle composition may contribute to the observed scavenging efficiency. The presence of FTIR-measurable submicrometer silicate and carbonate species during the 5 and 7−8 August 2003 rain events indicates that dust aerosol was present in the supermicrometer mode. This insoluble dust corresponds to an observed reduction in the scavenging efficiency of the supermicrometer mode during these rain events. During the 7−8 August 2003 rain event there was no detectable sulfate or ammonium and the aerosol was ∼70% organic by mass: scavenging was less efficient in the accumulation mode, indicating that hydrophobic organic species may have been concentrated in the 0.15−0.4 μm size range. During the rain event on 10 August 2003, an aerosol composed of ∼50% ammonium sulfate and ∼50% organic carbon had an increased scavenging efficiency from 0.25 to 0.5 μm, suggesting that there were increased concentrations of water-soluble ammonium sulfate in this size range. Composition-dependent variations may explain the large range of scavenging coefficients observed by Volken and Schumann (*4*), spanning 2 orders of magnitude at most of the measured particle diameters.

FTIR-measured aerosol concentrations for samples before, during, and after each of the three rain events of Figure 9 are shown in Figure 10. The effects of wet deposition are evident in this figure, with concentrations of all species decreasing as each rain event continued. The solution to the below-cloud scavenging equation for monodisperse aerosol and rain droplet populations, of the form $y = c_0 e^{-\lambda t}$, was used to fit the data with R^2 values above 0.5 in all cases except for silicate ($R^2 = 0.4$). The scavenging coefficients determined in this manner are 3 times larger for sulfate and ammonium than they are for OM and for silicate species, demonstrating preferential scavenging of the water-soluble inorganic species. The accuracy of the absolute values of the scavenging coefficients obtained from these curve fits is limited by the low temporal resolution of the FTIR data set and the inherent variability between the three rain events.

Focusing on the scavenging of OM, Figure 11 demonstrates that the water-soluble OM fraction decreased from approximately 60% to 20% from the beginning to the end of the three observed rain events. A linear fit to the nine data points from all three rain events has an intercept of 0.55 at $t = 0$, a slope of −0.001 min^{-1}, and an R^2 value of 0.77. An extrapolation of this linear fit suggests that a rain event lasting 9 h would result in a water-soluble OM fraction of close to 0%. The reduction in the hygroscopicity of submicrometer OM with time indicates that hydrophilic organic species may have been scavenged more efficiently than hydrophobic ones during the observed rain events.

FTIR data before and after the start of each rain event can provide chemical compositions for the scavenged and residual aerosol fractions. Of the three analyzed rain events, the largest aerosol mass concentrations and smallest percentage uncertainties were associated with the 10 August 2003 rain event, making it uniquely suited for such a scavenging analysis. The prerain aerosol composition 1.7 h before the start of precipitation on 10 August 2003 is shown in Figure 12, along with the chemical composition of the scavenged and residual aerosol fractions as measured 1.0 h after the start of precipitation. Sulfate, ammonium, and carbonyl functional groups are larger mass fractions of the scavenged aerosol relative to the residual aerosol. Conversely, hydrophobic organic functional groups are a larger fraction of the residual aerosol mass. This difference in chemical composition supports the preferential scavenging of hydrophilic functional groups reported above and suggests that a significant fraction of the hydrophilic and hydrophobic functional groups are externally mixed.

The preferential scavenging of hydrophilic organic compounds observed here has also been observed for cloud conditions by Raymond and Pandis (*23*). This scavenging behavior is consistent with an aerosol in which hydrophilic organic compounds are internally mixed with water-soluble inorganic compounds. Modeling studies by Ming and Russell (*24*) concluded that hydrophilic internally mixed sulfate and organic aerosol contributed 86% of the total fog droplet number concentration in the Po Valley during fog events in 1989 and 1998−1999, with the remainder of the droplets (only 14%) formed from hydrophobic organic aerosol particles. Recent smog chamber studies by Tolocka et al. (*25*) indicate that hydrophilic oligomeric organic molecules can be formed on acidic inorganic seed aerosol, providing a mechanism for the preferential partitioning of hydrophilic organic compounds to sulfate aerosol.

Effects of composition on below-cloud scavenging efficiency are not presently incorporated into global climate models (*26*), as the scavenging efficiency is assumed to be composition-independent (*5*). In-cloud scavenging, on the other hand, has been shown by numerous field measurements to depend on composition, with water-soluble species partitioning more strongly into cloud droplets than insoluble

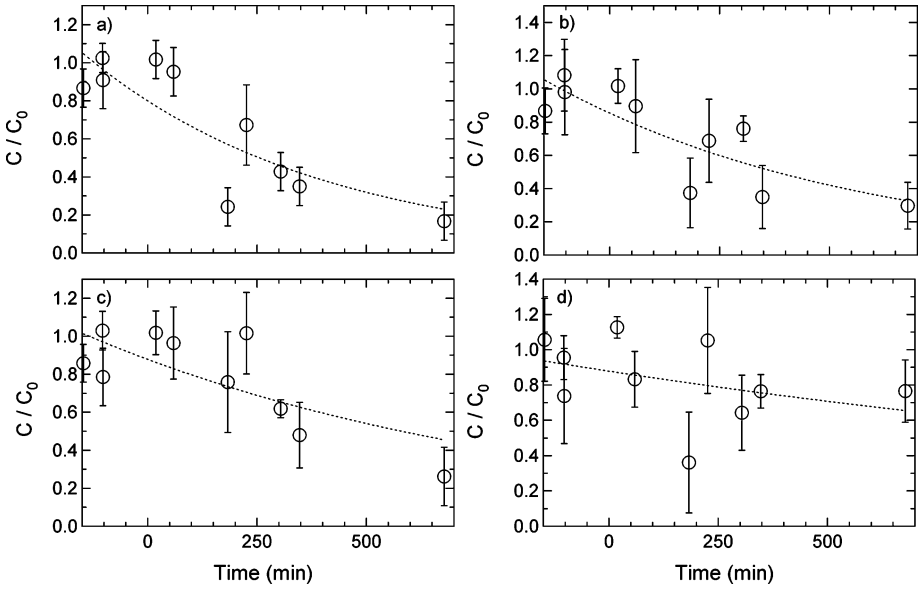

FIGURE 10. FTIR-measured aerosol concentration ratios of (a) sulfate, (b) ammonium, (c) OM, and (d) silicate immediately before, during, and immediately after rain events. Each concentration measurement is divided by the species concentration at the start of the corresponding rain event. Error bars indicate measurement uncertainty, and zero time corresponds to the start of each rain event. Curve fits of the form $y = c_0 e^{-\lambda t}$ are shown as dotted lines. The scavenging coefficients derived from these curve fits are 7.8×10^{-5} s^{-1} for sulfate (R^2 value of 0.8), 6.7×10^{-5} s^{-1} for ammonium (R^2 value of 0.7), 2.2×10^{-5} s^{-1} for OM (R^2 value of 0.7), and 7.2×10^{-6} s^{-1} for silicate (R^2 value of 0.1).

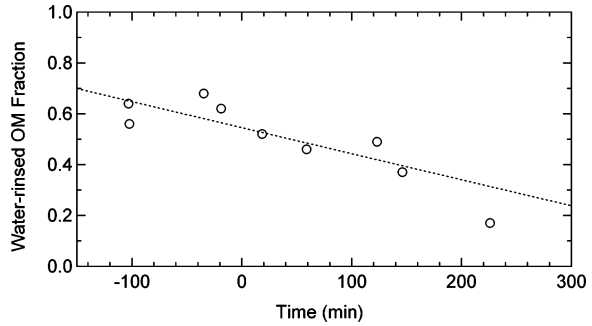

FIGURE 11. FTIR-measured water-rinsed OM fraction immediately before, during, and immediately after rain events. A linear fit to the data ($y = 0.55 - 0.001t$) is shown as a dotted line.

species (*27*, *28*). The composition dependence of the present data indicates that below-cloud scavenging during these rain events was affected by particle composition or that vertical mixing was allowing in-cloud scavenging to affect the measured aerosol concentrations. If below-cloud scavenging is composition-dependent, it is possible that Laakso et al. (*5*) and Volken and Schumann (*4*) did not observe this behavior because of the remoteness of their sampling sites. An aged aerosol sampled far from its source is likely to have undergone coagulation, a process that results in a well-mixed aerosol with little compositional heterogeneity. With either explanation, the ground-level aerosol concentrations are affected by chemically dependent processes that are not presently included in models of below-cloud scavenging.

For much of the 10-day aerosol sampling period, ambient aerosol concentrations remained below 10 μg m^{-3} due to the rainout from 10 rain events. FTIR-measured $PM_{1.0}$ concentrations were comparable to gravimetric $PM_{1.0}$ concentrations, with an average deviation of 1.2 μg m^{-3}. FTIR OM measurements identified a change in the aerosol organic composition at 9 August 2003, with larger alkene fractions in the motor vehicle-influenced aerosol prior to 9 August 2003 and larger alkane and amine fractions in the coal combustion-influenced aerosol after 9 August 2003. Throughout the sampling period, the aerosol was found to be

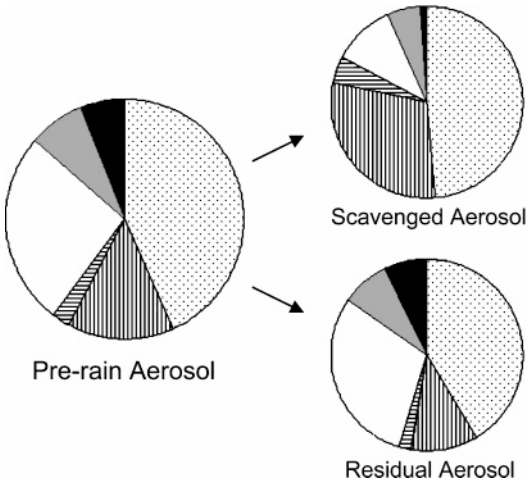

FIGURE 12. FTIR-measured $PM_{1.0}$ composition for aerosol collected 1.7 h before the start of the 10 August 2003 rain event (left). Also shown are the $PM_{1.0}$ compositions of the scavenged (top right) and residual (bottom right) aerosol fractions as determined from aerosol collected 1.0 h after the start of precipitation. Clockwise in each chart are mass fractions of sulfate (dotted), ammonium (vertically striped), carbonyl (horizontally striped), alkane (white), alkene (gray), and aromatic (black) functional groups. The mass fractions of all other functional groups are too small to be visible here. Particulate nitrate did not compose more than 1% of aerosol mass for these samples.

hydrophilic, with ~50% of OM removed in the water-rinsing analysis stage.

The scavenging coefficients calculated for three rain events demonstrate significant variations that appear to be related to aerosol chemical composition. Water-soluble sulfate and ammonium species were scavenged more efficiently than OM and silicate species. Water-soluble OM was also removed from the atmosphere more efficiently than hydrophobic OM, resulting in a water-soluble OM fraction that decreased throughout each rain event. These results show a relationship between chemical composition and aerosol scavenging. This relationship must be included in models of aerosol scavenging

in order to accurately predict atmospheric concentrations of aerosol species.

Acknowledgments

Support for this research was provided by the James S. McDonnell Foundation and by National Science Foundation Grant ATM-0408501. We thank Barbara J. Turpin, Robert J. Porcja, and the NIEHS Center of Excellence at EOHSI (Rutgers University) for use of the weighing facility and FTIR spectrometer.

Literature Cited

(1) Intergovernmental Panel on Climate Change. *Climate Change 2001—The Scientific Basis*; Cambridge University Press: New York, 2001.

(2) Zhang, L.; Michelangeli, D. V.; Taylor, P. A. Numerical studies of aerosol scavenging by low-level, warm stratiform clouds and precipitation. *Atmos. Environ.* **2004**, *38* (28), 4653−4665.

(3) Andronache, C. Estimated variability of below-cloud aerosol removal by rainfall for observed aerosol size distributions. *Atmos. Chem. Phys.* **2003**, *3*, 131−143.

(4) Volken, M.; Schumann, T. A critical review of below-cloud aerosol scavenging results on Mt. Rigi. *Water, Air, Soil Pollut.* **1993**, *68*, 15−28.

(5) Laakso, L.; Gronholm, T.; Rannik, U.; Kosmale, M.; Fiedler, V.; Vehkamaki, H.; Kulmala, M. Ultrafine particle scavenging coefficients calculated from 6 years field measurements. *Atmos. Environ.* **2003**, *37*, 3605−3613.

(6) Rasch, P. J.; Feichter, J.; Law, K.; Mahowald, N.; Penner, J.; Benkovitz, C.; Genthon, C.; Giannakopoulos, C,; Kasibhatla, P.; Koch, D.; Levy, H.; Maki, T.; Prather, M.; Roberts, D. L.; Roelofs, G.-J.; Stevenson, D.; Stockwell, Z.; Taguchi, S.; Kritz, M.; Chipperfield, M.; Baldocchi, D.; McMurry, P.; Barrie, L.; Balkanski, Y.; Chatfield, R.; Kjellstrom, E.; Lawrence, M.; Lee, H. N.; Lelieveld, J.; Noone, K. J.; Seinfeld, J.; Stenchikov, G.; Schwartz, S.; Walcek, C.; Williamson, D. A comparison of scavenging and deposition processes in global models: results from the WCRP Cambridge Workshop of 1995. *Tellus* **2000**, *52B*, 1025−1056.

(7) Maria, S. F.; Russell, L. M.; Turpin, B. J.; Porcja, R. J. FTIR measurements of functional groups and organic mass in aerosol samples over the Caribbean. *Atmos. Environ.* **2002**, *36*, 5185−5196.

(8) Maria, S. F.; Russell, L. M.; Turpin, B. J.; Porcja, R. J.; Campos, T. L.; Weber, R. J.; Huebert, B. J. Source signatures of carbon monoxide and organic functional groups in Asian Pacific Regional Aerosol Characterization Experiment (ACE-Asia) submicron aerosol types. *J. Geophys. Res.* **2003**, *108*, doi 10.1029/2003JD003703.

(9) Russell, L. M. Aerosol organic-mass-to-organic-carbon ratio measurements. *Environ. Sci. Technol.* **2003**, *37*, 2982−2987.

(10) Allen, D. T.; Palen, E. J.; Haimov, M. I.; Hering, S. V.; Young, J. R. Fourier transform infrared spectroscopy of aerosol collected in a low-pressure impactor (LPI/FTIR)—Method development and field calibration. *Aerosol Sci. Technol.* **1994**, *21*, 325−342.

(11) Martinez, J. R.; Ruiz, F.; Vorobiev, Y. V.; Perez-Robles, F.; Gonzalez-Henandez, J. Infrared spectroscopy analysis of the local atomic structure in silica prepared by sol−gel. *J. Chem. Phys.* **1998**, *109*, 7511−7514.

(12) Harrison, R. M.; Jones, A. M.; Lawrence, R. G. A pragmatic mass closure model for airborne particulate matter at urban background and roadside sites. *Atmos. Environ.* **2003**, *37*, 4927−4933.

(13) Maenhaut, W., Schwarz, J.; Cafmeyer, J.; Chi, X. G. Aerosol chemical mass closure during the EUROTRAC-2 AEROSOL Intercomparison 2000. *Nucl. Instrum. Methods Phys. Res., Sect. B* **2002**, *189*, 233−237.

(14) Henry, R. C.; Lewis, C. W.; Hopke, P. K.; Williamson, H. J. Review of receptor model fundamentals. *Atmos. Environ.* **1984**, *18*, 1507−1515.

(15) Lee, J. H.; Yoshida, Y.; Turpin, B. J.; Hopke, P. K.; Poirot, R. L.; Lioy, P. J.; Oxley, J. C. Identification of sources contributing to Mid-Atlantic regional aerosol. *J. Air Waste Manage. Assoc.* **2002**, *52*, 1186−1205.

(16) Draxier, R. R.; Hess, G. D. An overview of the $HYSPLIT_4$ modelling system for trajectories, dispersion and deposition. *Aust. Meteor. Magn.* **1998**, *47*, 295−308.

(17) Schauer, J. J.; Kleeman, M. J.; Cass, G. R.; Simoneit B. R. T. Measurement of emissions from air pollution sources. 2. C-1 through C-30 organic compounds from medium duty diesel trucks. *Environ. Sci. Technol.* **1999**, *33*, 1578−1587.

(18) Schauer, J. J.; Kleeman, M. J.; Cass, G. R.; Simoneit B. R. T. Measurement of emissions from air pollution sources. 5. C-1−C-32 organic compounds from gasoline-powered motor vehicles. *Environ. Sci. Technol.* **2002**, *36*, 1169−1180.

(19) Ming, Y.; Russell, L. M. Predicted hygroscopic growth of sea salt particles. *J. Geophys. Res.* **2001**, *106*, 28259−28274.

(20) Claassen, H. C.; Halm, D. R. A possible deficiency in estimates of wet deposition obtained from data generated by the NADP/NTN network. *Atmos. Environ.* **1995**, *29*, 437−448.

(21) Dana, M. T.; Hales, J. M. Statistical aspects of washout of polydisperse aerosols. *Atmos. Environ.* **1976**, *10*, 45−50.

(22) Seinfeld, J. H.; Pandis, S. N. *Atmospheric Chemistry and Physics: From Air Pollution to Climate Change*; John Wiley and Sons: New York, 1997.

(23) Raymond, T. M.; Pandis, S. N. Cloud activation of single-component organic aerosol particles. *J. Geophys. Res.* **2002**, *107*, doi 10.1029/2002JD002159.

(24) Ming, Y.; Russell, L. M. Organic aerosol effects on fog droplet spectra. *J. Geophys. Res.* **2004**, *109*, doi 10.1029/2003JD004427.

(25) Tolocka, M. P.; Jang, M.; Ginter, J. M.; Cox, F. J.; Kamens, R. M.; Johnston, M. V. Formation of oligomers in secondary organic aerosol. *Environ. Sci. Technol.* **2004**, *38*, 1428−1434.

(26) Guelle, W.; Balkanski, Y. J.; Schulz, M.; Dulac, F.; Monfray, P. Wet deposition in a global size-dependent aerosol transport model 1. Comparison of a 1 year Pb-210 simulation with ground measurements. *J. Geophys. Res.* **1998**, *103*, 11429−11445.

(27) Hitzenberger, R.; Berner, A.; Kromp, R.; Kasper-Giebl, A.; Limbeck, A.; Tscherwenka, W.; Puxbaum, H. Black carbon and other species at a high-elevation European site (Mount Sonnblick, 3106 m, Austria): Concentrations and scavenging efficiencies. *J. Geophys. Res.* **2000**, *105*, 24637−24645.

(28) Limbeck, A.; Puxbaum, H. Dependence of in-cloud scavenging of polar organic aerosol compounds on the water solubility. *J. Geophys. Res.* **2000**, 105, 19857−19867.

Received for review June 3, 2004. Revised manuscript received March 8, 2005. Accepted April 13, 2005.

ES0491679